Carbohydrate Polymers 84 (2011) 669–676

Contents lists available at ScienceDirect

Carbohydrate Polymers

journal homepage: www.elsevier.com/locate/carbpol

The effect of calcium salts on the viscosity and adsorption behavior of xanthan

Aline F. Dário[a], Lucas M.A. Hortêncio[a], Maria Rita Sierakowski[b], João C. Queiroz Neto[c], Denise F.S. Petri[a,*]

[a] Instituto de Química, Universidade de São Paulo, Av. Prof. Lineu Prestes 748, 05508-000 São Paulo, SP, Brazil
[b] BioPol, Departamento de Química, Universidade Federal do Paraná, Curitiba, PR, Brazil
[c] Centro de Pesquisas da PETROBRAS, Rio de Janeiro, RJ, Brazil

ARTICLE INFO

Article history:
Received 13 September 2010
Received in revised form 9 December 2010
Accepted 16 December 2010
Available online 23 December 2010

Keywords:
Xanthan gum
Calcium salts
Flow behavior
Adsorption
AFM

ABSTRACT

The effect of $CaCl_2$, $Ca(NO_3)_2$, $CaSO_4$, $CaCO_3$ and $Ca_3(PO_4)_2$ on the flow behavior of xanthan gum solutions was investigated. Regardless the concentration and type of calcium salt used, xanthan solutions presented pseudoplastic behavior. The soluble salts ($CaCl_2$ and $Ca(NO_3)_2$) induced the disordered state in the xanthan chains at concentration of 1.0 g/L or 10 g/L, decreasing the flow consistency index (*K*) values. At 100 g/L soluble salts *K* values were similar to those found for pure xanthan solutions, whereas at the same concentration of insoluble particles the *K* values increased 20%. The adsorption of xanthan gum onto Si/SiO_2 surfaces in the presence of calcium salts was investigated by ellipsometry and atomic force microscopy (AFM). The adsorbed layer of xanthan onto Si/SiO_2 consisted of two regions: (i) a thin acid resistant sublayer, where xanthan chains were like highly entangled fibers and (ii) a thick upperlayer, whose morphology was calcium salt dependent.

1. Introduction

Xanthan gum is a biopolymer with branched chains, anionic characteristics and molecular weight of approximately 2 million g/mol (Rosalam & England, 2006). It is obtained from the microbiological fermentation in aerobic conditions of sugar cane, corn or their derivatives, which are transformed into a soluble gum during the reaction in the presence of the bacterium *Xanthomonas campestris*. The resultant gum turns into xanthan gum powder, by precipitation in a non-soluble solvent. Xanthan gum consists of D-glucosyl, D-mannosyl, and D-glucuronyl acid residues in a 2:2:1 molar ratio and variable proportions of *O*-acetyl and pyruvyl residues. It is an acidic polymer consisting of pentasaccharide subunits, forming a cellulose backbone with trisaccharide side-chains composed of mannose (β-1,4) glucuronic acid (β-1,2) mannose attached to alternate glucose residues in the backbone by α-1,3 linkages, as schematically represented in Supplementary material SM1. A ketal linkage joined by a pyruvic acid moiety is on approximately half of the terminal mannose residues. Acetyl groups are often present as 6-*O* substituents on the internal mannose residues. Due to its rheological properties and thermal stability below 100 °C, it has been used in drilling fluid (Chilingarian & Vorabutr, 1981) food and cosmetic formulations (Geremia & Rinaudo, 2005). Xanthan gum yields high viscosities at low shear rates and stabilizes suspensions, while providing good flow properties when poured or spooned from a container. At the processing stage, low viscosity at high shear rates allows xanthan gum solutions to be easily pumped and poured. Xanthan gum is characterized by its very high viscosity at low concentrations. Because of its pseudoplastic nature, it also imparts excellent stability to oil-in-water emulsions by preventing the oil droplets from coalescing.

Temperature and ionic strength of the medium control the equilibrium between the ordered and disordered states for xanthan chains in aqueous solution, as reported in the literature (Born, Langendorff, & Boulenguer, 2002; Gravanis, Milas, Rinaudo, & Tinland, 1987; Liu, Sato, Norisuye, & Fujita, 1987; Milas, Rinaudo, Duplessix, Borsali, & Lindner, 1995; Milas, Reed, & Printz, 1996; Muller, Anrhourrache, Lecourtier, & Chauveteau, 1986; Symes, 1980; Tinland & Rinaudo, 1989; Xie & Lecourtier, 1992). Under low ionic strength or high temperature, more flexible structures (i.e., the disordered state) with persistence length of ~50 Å are expected. On the other hand, under high ionic strength or low temperature, xanthan chains tend to assume single or double helix conformations with persistence length of ~350 Å (Tinland & Rinaudo, 1989). This information is especially important for formulation purposes, because rheological properties are strongly dependent on the xanthan conformational state and stiffness (Renaud, Belgacem, & Rinaudo, 2005).

The *O*-acetyl and pyruvyl residues in the xanthan side chains provides conditions for complexation with bivalent cations. Conductometric, viscometric titrations and nuclear magnetic reso-

* Corresponding author. Tel.: +55 11 30913831; fax: +55 11 3815 5579.
E-mail address: dfsp@iq.usp.br (D.F.S. Petri).

0144-8617/$ – see front matter © 2010 Elsevier Ltd. All rights reserved.
doi:10.1016/j.carbpol.2010.12.047

nance spectroscopy revealed that a single bivalent cation forms a complex, which involves two disaccharide units of the main chain and two carboxylate groups at side chains, leading to intramolecular cross-linking and chains contraction. Moreover, heavy metal ions (Cd^{2+} and Pb^{2+}) presented stronger binding to the xanthan chain than lighter cations (Ca^{2+} and Mg^{2+}) (Bergmann, Furth, & Mayer, 2008). The gel-like behavior of xanthan was investigated as a function of temperature and $CaCl_2$ concentration. Solutions passed through states of maximum and minimum gel-like character at 100% and 200% stoichiometric equivalence of Ca^{2+}, which were ascribed to the partial replacement of intermolecular site-binding of calcium ions by binding to individual carboxyl groups, maximizing the degree of complexation and network formation (Mohammed, Haque, Richardson, & Morris, 2007). The use of Ca^{2+} ions as chelating agents was applied for xanthan chains and for other charged polysaccharides, such as alginate (Draget, Braek, & Smidsrod, 1994) and hyaluronic acid (Furth, Knierim, Buss, & Mayer, 2008). In this work, we investigated the effect of soluble ($CaCl_2$ and $Ca(NO_3)_2$) and insoluble ($CaSO_4$, $CaCO_3$, $Ca_3(PO_4)_2$) calcium salts on the flow behavior of xanthan gum solutions. Moreover, the adsorption of xanthan gum onto Si/SiO_2 surfaces in the presence of calcium salts (soluble and insoluble) was investigated by means of ellipsometry and atomic force microscopy (AFM).

2. Materials and methods

Si/SiO_2 wafers purchased from Wafers University (Massachusetts, USA) with a native oxide (SiO_2) layer approximately 2 nm thick were cut into peaces of approximately 1 cm^2 and rinsed as described elsewhere (Fujimoto & Petri, 2001). $CaCl_2$, $Ca(NO_3)_2$, $CaSO_4$, $CaCO_3$ and $Ca_3(PO_4)_2$ were analytical grade (LabSynth, São Paulo, Brazil) and used without further purification. The insoluble $CaSO_4$, $CaCO_3$ and $Ca_3(PO_4)_2$ particles were analyzed by means of scanning electron microscopy in a JEOL SEM-FEG 7401 equipment. SEM images presented as Supplementary material (SM2) revealed that dried $CaSO_4$, $CaCO_3$ and $Ca_3(PO_4)_2$ particles present distinguished morphologies. $CaSO_4$ particles appeared as large crystals, $CaCO_3$ presented large aggregates of small particles and $Ca_3(PO_4)_2$ particles are large structures formed by tiny grains. However, should notice that such structures are observed prior to use and they are probably destroyed under shear during dispersion preparation in the mechanical stirrer, as described below.

Commercial xanthan (Kelzan®, CP Kelco, USA, degree of pyruvate = 0.38, degree of acetyl = 0.41, $M_v \sim 1 \times 10^6$ g/mol, degree of polymerization ~ 1072) was used as received. Xanthan solutions (4.0 g/L) were prepared at (24 ± 1) °C and pH 10. This xanthan concentration was chosen because it is well above the dilute regime, which is below 0.25 g/L (Cuvelier & Launay, 1986), and is typically used in drilling fluid formulations. Alkaline conditions (pH 10) were chosen because they allow high charge density on the xanthan chains and on the Si/SiO_2 surfaces. Soluble and insoluble calcium salts were added in the concentration range of 1.0–100 g/L (Table 1). All systems were prepared with a Harlibuton® mechanical stirrer.

Apparent viscosity (μ_{ap}) was determined with a Fann viscometer model 35 A (R1-B1 cylinders set) at (24 ± 1) °C, at the shear rates (γ) 5.1 s^{-1}, 10.2 s^{-1}, 170.3 s^{-1}, 340.6 s^{-1}, 511 s^{-1} and 1022 s^{-1}. Although the experimental conditions are limited to the shear range convenient for petroleum operational units, they are useful for evaluating the effect of different calcium salts on the flow behavior of xanthan solutions in this study.

Adsorption experiments were carried out by dipping Si/SiO_2 wafers into the xanthan gum and calcium salts solutions. The wafers remained in the solution for 24 h at (24 ± 1) °C. Afterwards, half of the samples was rinsed with distilled water and dried under a N_2 stream. The rest of the samples was immersed into HCl (1.0 mol/L) for 30 min, rinsed with distilled water and dried under a N_2 stream. Rinsing with distilled water or HCl was important to removing the physically adsorbed material.

Ellipsometric measurements were performed in air using a vertical computer-controlled DRE-EL02 ellipsometer (Ratzeburg, Germany). The angle of incidence was set at 70.0° and the wavelength, λ, of the He–Ne laser was 632.8 nm. For data interpretation, a multilayer model composed of the substrate, the unknown layer, and the surrounding medium were used. The thickness, d_x, and refractive index, n_x, of the unknown layer were calculated from the ellipsometric angles, Δ and Ψ, using the fundamental ellipsometric equation and iterative calculations with Jones matrices (Azzam & Bashara, 1987):

$$e^{i\Delta} \times \tan \Psi = \frac{R_p}{R_s} = f(n_x, d_x, \lambda, \phi) \quad (1)$$

where R_p and R_s are the overall reflection coefficients for the parallel and perpendicular waves, which are functions of the angle of incidence, ϕ, the wavelength of the radiation, λ, and of the refractive index and thickness of each layer of the model, n_x and d_x, respectively.

From the ellipsometric angles, Δ and Ψ, and a multilayer model composed of silicon, silicon dioxide, polysaccharide layer, and air, it is possible to determine only the thickness of the xanthan layer, $d_{xanthan}$. The thickness of the silicon dioxide layers was determined in air, assuming a refractive index of 3.88–0.018i and infinite thickness for silicon (Palik, 1985). The refractive index for the surrounding medium (air) was taken as 1.00. Because the native silicon dioxide layer is very thin, its refractive index was taken as 1.462 (Palik, 1985) and only its thickness was calculated. The mean thickness of the native silicon dioxide layer was (2.0 ± 0.2) nm. After determining the thickness of the silicon dioxide layer, the mean thickness and index of refraction of the adsorbed xanthan layers were determined independently in air by means of ellipsometry.

Atomic force microscopy (*AFM*) analyses were performed with a PICO SPM-LE (Molecular Imaging) microscope in intermittent contact mode in air at room temperature, using silicon cantilevers with a resonance frequency close to 300 kHz. Areas 1 μm × 1 μm were scanned with a resolution of 512 × 512 pixels. Image processing and the determination of the root mean square (rms) roughness values were performed using the Pico Scan software. At least three films of the same composition were analyzed in different areas of the surface.

3. Results and discussion

3.1. Viscosity of xanthan solutions

The flow curves obtained for pure xanthan solution (Supplementary material SM3) could be fitted with an exponential decay, while the viscosity curves presented typical shear thinning behavior (Supplementary material SM4), as expected for xanthan solution. The viscosity decreased from (750 ± 50) mPa s (at 5.1 s^{-1}) to (17 ± 1) mPa s (at 1022 s^{-1}). At low shear rates or at rest the high viscosity is attributed to the existence of an ordered rod-like conformation with high persistence length (~40 nm) (Tinland & Rinaudo, 1989), which can self-associate creating non-permanent aggregates. Such aggregates are disrupted upon increasing the shear rate, decreasing the viscosity.

The viscosity curves were fitted with the empirical power law model (Barnes, Hutton, & Walters, 1989), which predicts the linear dependence of log (viscosity) with log (shear rate):

$$\log \mu_{ap} = \log K + (n-1) \log \gamma \quad (2)$$

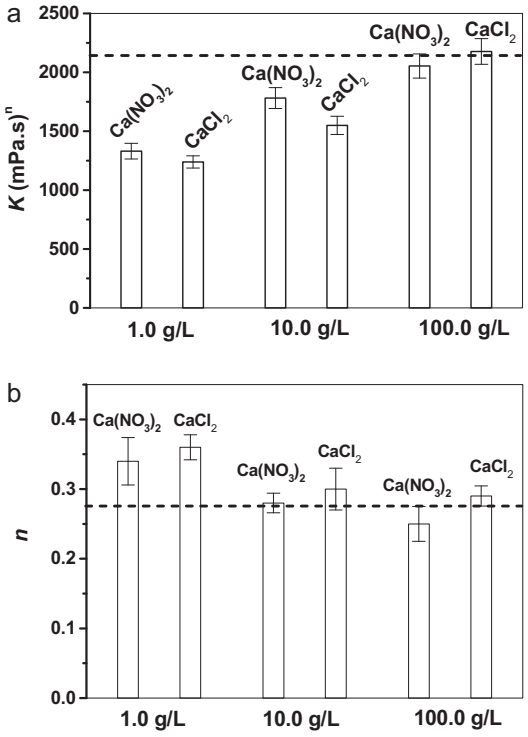

Fig. 1. (a) Flow consistency index (K) and (b) flow behavior index (n) determined for xanthan solutions in the presence of $Ca(NO_3)_2$ or $CaCl_2$, at (24 ± 1) °C and pH 10. The dash lines in (a) and in (b) correspond to K and n values, respectively, determined for pure xanthan solution.

or

$$\mu_{ap} = K\gamma^{(n-1)} \quad (3)$$

where K (Pa s^n) is the flow consistency index, which is related to the material resistance to change of shape, and n is the flow behavior index. If $n = 1$, fluid has Newtonian behavior, while $n < 1$ indicates pseudoplastic behavior.

The dependence of $\log(\mu_{ap})$ with $\log(\gamma)$ along with the linear fit determined for pure xanthan solution at 4.0 g/L (Supplementary material SM5) yielded the mean fitting parameters K and n, obtained from triplicates. These values were substituted in Eq. (3):

$$\mu_{ap} = (2137 \pm 53)\,\text{mPa s}^{0.27\pm0.03}(\gamma)^{-0.73\pm0.03}$$

The small n value (0.27 ± 0.03) confirms the pseudoplastic behavior of xanthan solution.

The addition of soluble calcium ions did not change the shear thinning behavior observed for pure xanthan gum solutions (flow and viscosity curves in Supplementary material SM6 and SM7, respectively). The fitting parameters K and n determined from a linear fit for the dependence of $\log(\mu_{ap})$ on $\log(\gamma)$ varied with salt concentration, as shown in Fig. 1a and b, respectively.

Comparing the effects observed in the presence of $CaCl_2$ and $Ca(NO_3)_2$, one notices that the type of anion (Cl^- or NO_3^-) had no significant effect on K and n values. This can be explained by their similar ionic hydration enthalpies, namely, −381 kJ/mol and −314 kJ/mol, for Cl^- and NO_3^-, respectively (Smith, 1977). On the other hand, K and n values were influenced by the amount of salt added to xanthan solutions. The addition of low amounts (1.0 g/L) of soluble calcium salts to xanthan solutions (4 g/L) led to a decrease of K values and increase of n values (Fig. 1a and b, respectively). However, the increase of K and the decrease of n values were observed for solutions containing high amounts (10 g/L or 100.0 g/L) of $Ca(NO_3)_2$ or $CaCl_2$ (Fig. 1a and b). Such behavior is due to the xanthan ordered–disordered transition brought about by ionic strength changes. At low ionic strength xanthan chains are expected to be in the disordered state, which causes decrease of K and increase of n. Upon increasing the ionic strength xanthan chains become ordered, increasing K and decreasing n (Milas et al., 1995; Born et al., 2002).

Recently, the effect of calcium ions on the rheology of xanthan was studied by low-amplitude oscillatory measurements (Mohammed et al., 2007). Starting from ordered conformation the addition of Ca^{2+} at the 100% stoichiometric equivalence led to gel-like state, which was disrupted when Ca^{2+} ions concentration was increased to 200% stoichiometric equivalence. Such effect was attributed to the partial replacement of the intermolecular site-binding of calcium ions by binding to individual carboxyl groups. In the present system the number of negative charges stemming from xanthan carboxyl groups (solution at 4 g/L) was estimated as $\sim 2 \times 10^{21}$ considering the degree of polymerization ~1072, degree of pyruvate of 0.38 and degree of acetyl of 0.41. The stoichiometric equivalence should be reached when Ca^{2+} ions solutions are at 1.0 g/L $Ca(NO_3)_2$ or $CaCl_2$, which yield $\sim 7 \times 10^{21}$ and 10×10^{21} positive charges respectively. The high shear rates, characteristic of the Fann viscometer, do not allow analyzing any gel state, because the sample is immediately disrupted under shear. However, the xanthan structure seems to be more stable when the salt concentration was 10.0 g/L or 100 g/L, because consistency increased considerably. Literature reports have shown that salt induced xanthan conformation stabilization, since the order–disorder transition temperature is higher when the ionic strength is enhanced (Xie & Lecourtier, 1992).

For some industrial applications inorganic water insoluble particles are added to xanthan gum solutions to increase viscosity (Chilingarian & Vorabutr, 1981). Calcium carbonate is used as weighting agent due to its high specific gravity (see Table 1) and relative low cost. In the present work, the effect of the type of insoluble calcium salt on the flow behavior of xanthan solution was investigated. The addition of $CaCO_3$ or $CaSO_4$ or $Ca_3(PO_4)_2$ to xanthan gum solutions did not change the shear thinning behavior observed for pure xanthan gum solutions (see Supplementary material SM8–SM11). The fitting parameters K and n determined from linear fit for the dependence of $\log(\mu_{ap})$ on $\log(\gamma)$ varied with particle concentration, as shown in Fig. 2a and b, respectively.

The addition of $CaSO_4$ exerted no significant effect on the K values of xanthan solution, regardless the concentration (Fig. 2a), but decreased the n values of xanthan solutions up to 20% (Fig. 2b), indicating that $CaSO_4$ favors the pseudoplastic behavior of xanthan solutions. In the case of $CaCO_3$, the K value was about half

Table 1
Calcium salts solubility and density (Weast, 1984) at 25 °C and concentration range of the xanthan solution.

Salt	Solubility in water (g/L)	Density (g/cm^3)	Concentration (mol/L)	Range (g/L)
$Ca(NO_3)_2$	1210	2.504	0.006–0.60	1.0–100
$CaCl_2$	745	2.15	0.009–0.9	1.0–100
$CaSO_4$	2.1	2.61	0.007–0.7	1.0–100
$Ca_3(PO_4)_2$	0.020	3.14	0.003–0.32	1.0–100
$CaCO_3$	0.014	2.93	0.001–1.0	1.0–100

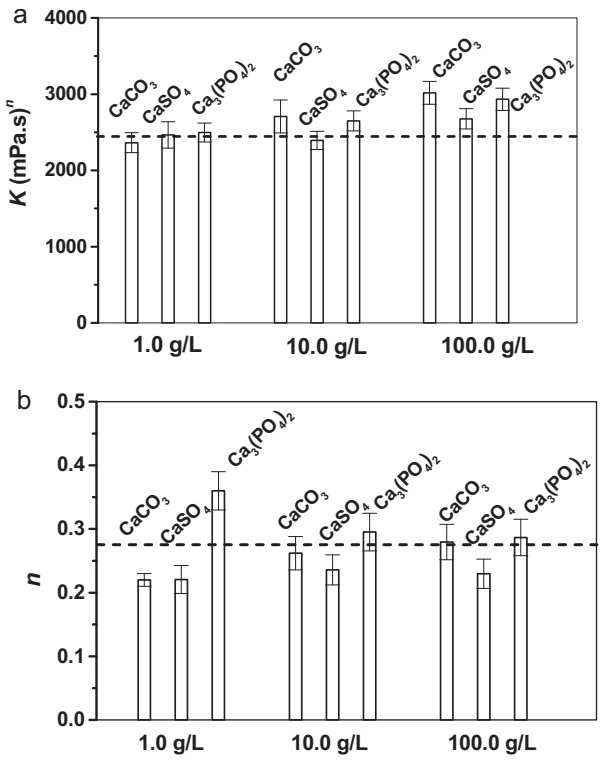

Fig. 2. (a) Flow consistency index (K) and (b) flow behavior index (n) determined for xanthan solutions in the presence of $CaCO_3$ or $CaSO_4$ or $Ca_3(PO_4)_2$, at (24 ± 1) °C and pH 10. The dash lines in (a) and in (b) correspond to K and n values, respectively, determined for pure xanthan solution.

of that determined for pure xanthan solution when the concentration was 1.0 g/L (Fig. 2a), indicating that a small amount of particles induced the disordered state in xanthan chains. At 10 g/L or 100 g/L of $CaCO_3$ the K value increased by 10% and 20%, respectively, of that observed for pure xanthan solution. Nevertheless, the addition of $CaCO_3$ had no significant effect on the n values of xanthan solutions (Fig. 2b). The K value determined for xanthan solution was not affected by small amount (1.0 g/L) of salt, but solutions containing 10 g/L or 100 g/L of $Ca_3(PO_4)_2$ exhibited increases in the K value of ~10% and 20%, respectively. These findings might be explained by the density values of $CaCO_3$ and $Ca_3(PO_4)_2$, which are the largest among the salts studied here. Considering Einstein's principle that the viscosity of dilute suspensions of non-interacting rigid spheres increases with the dispersed phase volume fraction, higher particle density values yield smaller volume fraction and, therefore, the viscosity should decrease with increasing particle density. However, the systems studied here comprise particles, which interact with the medium (xanthan solution) and for this reason Einstein's principle is not longer valid. On the other hand, the increase of density increases the hydrostatic pressure exerted by system, and consequently the internal friction, which increases the viscosity. The addition of $Ca_3(PO_4)_2$ to the xanthan solutions disfavored the pseudoplastic behavior, regardless the particle concentration (Fig. 2b). Another important characteristic is the water bound to the particle surface. Considering that hydration is favored for large charge/ionic radius ratio, the surface of $Ca_3(PO_4)_2$ particles should be more hydrated than the surface of $CaCO_3$ or $CaSO_4$ particles. Although the addition of 100 g/L $CaCO_3$ or $Ca_3(PO_4)_2$ corresponds to a small volume fraction (~0.035) of solid particle in the dispersion, it is enough to increase the K values of xanthan solutions by 20%, keeping the pseudoplastic behavior. Xanthan chains bind to the surface of insoluble calcium particles possibly building a network as suggested in Supplementary material SM12. The flow behavior of such network clearly depends on the degree of hydration of particles surfaces, since the most hydrate counter-ions (phosphate) led to the highest flow index (K) values.

So far the effect of calcium salts on the flow behavior of xanthan solutions can be summarized as follows. The pseudoplastic behavior of xanthan solutions was observed in the presence of all calcium salts, regardless the concentration. The soluble salts induced the disordered state in the xanthan chains when the concentration was 1.0 g/L or 10 g/L, decreasing the K values. However, when the salt concentration was 100 g/L K values were similar to those found for pure xanthan solutions, indicating the recovery of ordered state induced by the high ionic strength. The addition of 100 g/L insoluble $CaCO_3$ or $Ca_3(PO_4)_2$ particles increased the K values of xanthan solutions by 20%, which might be an important effect for commercial formulations. Smaller amounts of insoluble particles exerted no significant effect on the K values. The weaker effect of $CaSO_4$ on the flow behavior of xanthan solutions might be attributed to the lower particle density.

3.2. Adsorption behavior of xanthan gum onto Si/SiO_2 surfaces in the presence of calcium salts

The mean thickness and index of refraction of the adsorbed xanthan gum layers ($d_{xanthan}$) amounted to (17 ± 3) nm and (1.53 ± 0.01), respectively. After acidic treatment $d_{xanthan}$ decreased to (10 ± 4) nm. The large error on measurements is due to the inhomogeneous adsorbed layer, which remained after rinsing with water or HCl. The topographic AFM images obtained for the xanthan gum layer adsorbed onto Si/SiO_2 wafers reveal a well-packed layer with some fibers and small aggregates (white spots) (Fig. 3a). Upon adsorbing, the xanthan chains formed smooth (rms = 0.5 ± 0.1 nm) thick layers on the Si/SiO_2 wafers; for comparison bare Si/SiO_2 wafers present rms values $\sim 0.09 \pm 0.02$ nm. Treatment with HCl 1.0 mol/L caused fibers desorption (Fig. 3b) and mean roughness (rms) increase from 0.5 ± 0.1 nm to 1.2 ± 0.1 nm. The desorption of physically adsorbed xanthan chains by acidic rinsing increased the layers inhomogeneity. The adsorption constant was determined for xanthan onto SiO_2 at pH 7 as 910×10^6 L/mol, evidencing the strong interaction mediated by hydrogen bonding among xanthan hydroxyl groups and silanol groups (Neto, Biscaia, & Petri, 2007; Petri & Queiroz Neto, 2010).

The xanthan gum layers adsorbed from solutions containing either $Ca(NO_3)_2$ or $CaCl_2$ presented similar characteristics. At 1.0 g/L salt the mean thickness value determined for the adsorbed layer amounted to (19 ± 4) nm. However, at 10 g/L or 100 g/L salt it increased to (32 ± 5) nm. Such differences might be correlated with the disorder–order transition state, which is expected to occur upon increasing the ionic strength, as seen in flow consistency indices (K) in Fig. 1b. The large standard deviations are due to the lack of layer homogeneity. The topographic AFM images obtained for pure xanthan layer adsorbed in the presence of $Ca(NO_3)_2$ or $CaCl_2$ (not shown because they are similar to those of xanthan layer adsorbed in the presence of $Ca(NO_3)_2$) onto Si/SiO_2 wafers (Fig. 4) revealed that (i) regardless the salt amount no fiber is observed on the surfaces; (ii) the layer adsorbed at 1.0 g/L (Fig. 4a) is smoother (rms = 0.6 ± 0.1 nm) than that adsorbed at higher ionic strength (Fig. 4b, rms = 1.0 ± 0.1 nm); (iii) tiny aggregates appeared more frequently when the salt concentration was 10.0 g/L or 100.0 g/L (Fig. 4b), explaining the increase in the mean roughness; (iv) after treatment with 1.0 mol/L HCl thin fibers connected by small aggregates appeared on the surface (Fig. 4c), corroborating with the thickness decrease observed by ellipsometry and the small increase in the roughness values to 1.2 ± 0.1 nm. After acidic treatment the thickness values were reduced to approximately the half of the original values, indicating that the thick layer was built as a network of xanthan chains "chelated" by Ca^{2+} ions, which is destroyed

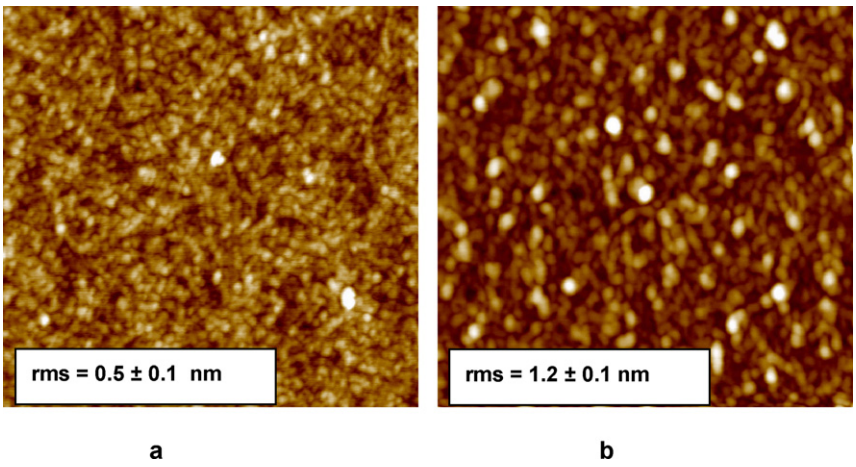

Fig. 3. AFM topographic images (1 μm × 1 μm) obtained for xanthan gum layer adsorbed onto Si/SiO_2 wafers (a) before treatment with HCl 1.0 mol/L, $Z = 4.0$ nm; (b) after treatment with HCl 1.0 mol/L, $Z = 10.0$ nm.

under acidic conditions. Moreover, the partial dissolution of this network revealed an underlayer rich in fibers, which were not visible before acid treatment. The fibers are ~1.0 nm high, as shown by the cross section analyses in Fig. 4d (arrows). These dimensions are in agreement with literature data, where the mean height of xanthan gum onto mica surface was determined as (1.12 ± 0.20) nm and were attributed to mono – or double layers (Iijima, Shinozaki, Hatakeyama, Takahashi, & Hatakeyama, 2007).

Considering that the addition of 100 g/L insoluble particles led to the most interesting flow behavior, adsorption experiments were performed only at this particle concentration. Fig. 5a shows the topographic image of adsorbed xanthan layer in the presence of $CaSO_4$, which evidences the formation of a network with many aligned xanthan chains. The mean thickness values was determined from ellipsometric measurements as (7 ± 1) nm. Although $CaSO_4$ particles weakly affected the flow behavior of xanthan solutions, the structures formed after adsorption (Fig. 5a) was more ordered than those observed for pure xanthan layer, despite of the similar rms values $(0.5 \pm 0.1$ nm). After the acid treatment the layer thickness was (4 ± 1) nm and a highly porous structure could be

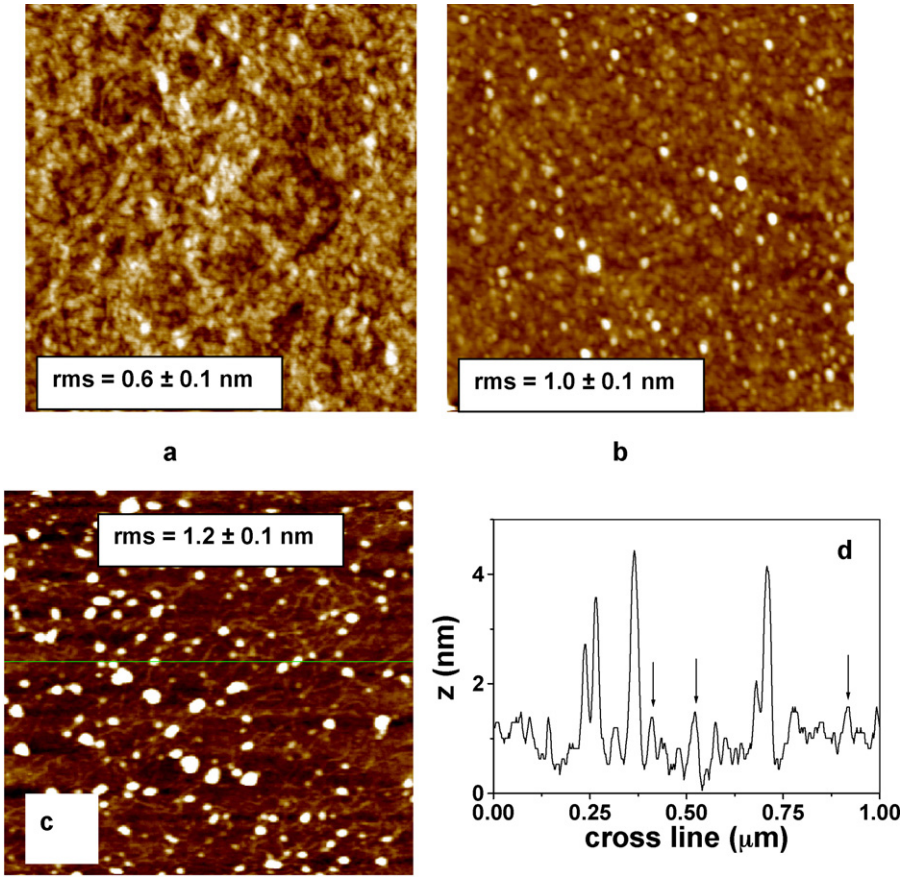

Fig. 4. Topographic AFM images (1 μm × 1 μm) obtained for xanthan layer adsorbed onto Si/SiO_2 wafers (a) in the presence of $Ca(NO_3)_2$ (1.0 g/L), $Z = 5.0$ nm, (b) in the presence of $Ca(NO_3)_2$ (10.0 g/L), $Z = 10.0$ nm, (c) in the presence of $Ca(NO_3)_2$ (100.0 g/L) after rinsing with HCl, $Z = 15.0$ nm and (d) the corresponding cross-section.

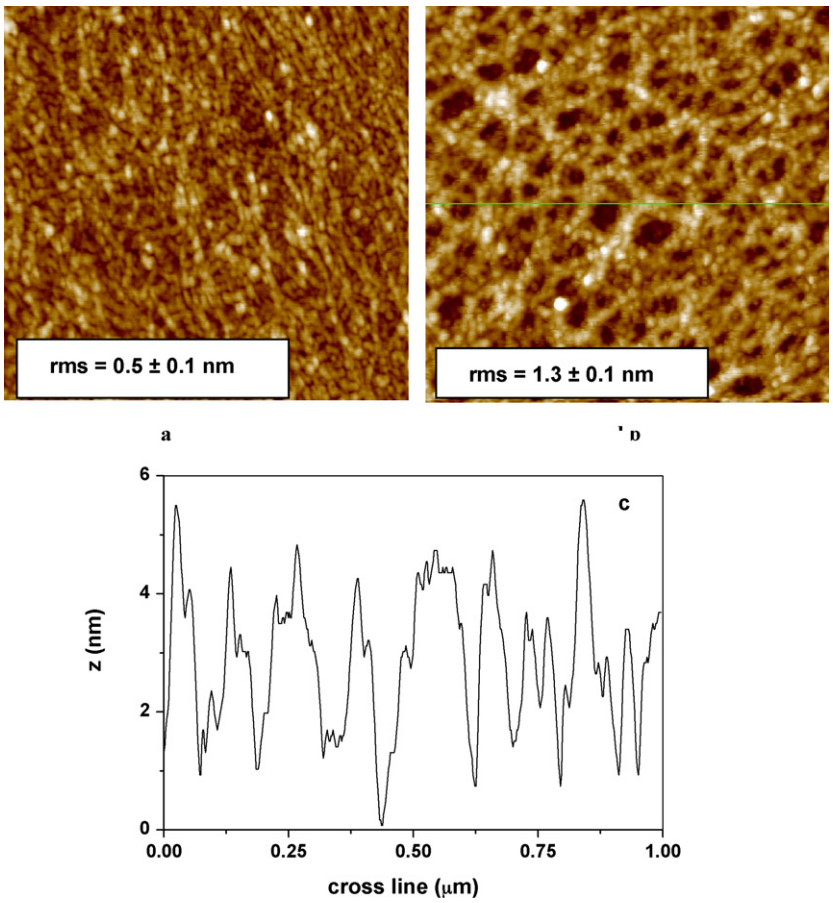

Fig. 5. Topographic AFM images (1 μm × 1 μm) obtained for xanthan layer adsorbed onto Si/SiO_2 wafers (a) in the presence of $CaSO_4$ (100.0 g/L), $Z = 6.0$ nm, (b) in the presence of $CaSO_4$ (100.0 g/L), after rinsing with HCl, $Z = 10.0$ nm and (c) the corresponding cross-section.

observed (Fig. 5b), which increased the rms values to (1.3 ± 0.1) nm). The pores probably correspond to the space originally occupied by $CaSO_4$ particles not bound to xanthan layers, which were dissolved by HCl. The remaining structure probably corresponds to the network formed by interconnected xanthan chains. The cross section in Fig. 5c shows that the pores are (4 ± 1) nm deep. Although it coincides with the mean layer thickness determined by means of ellipsometry, the deepest points do not correspond to the Si/SiO_2 surface, because material can still be seen inside the pores (Fig. 5b). One should notice that surface tension effects might also induce such structures during the drying procedure.

The topographic images of adsorbed xanthan layer in the presence of $CaCO_3$ and $Ca_3(PO_4)_2$ particles are shown in Figs. 6 and 7a, respectively. Although both types of particles increased the K values of xanthan by 20% in comparison to pure xanthan solution K value, the structures of xanthan layers adsorbed in the presence of each salt were quite different. The layer adsorbed in the presence of $Ca_3(PO_4)_2$ was (8 ± 1) nm thick and presented many entangled fibers (Fig. 6a). The corresponding cross section analyses (Fig. 6b) indicate that the layer is formed by thick $(2.0 \pm 0.5$ nm) and thin $(1.0 \pm 0.2$ nm) entangled fibers. Such structures were partially removed by HCl, as the mean thickness decreased to (5 ± 1) nm and rms values increased from (0.5 ± 0.1) nm (Fig. 6a) to (0.9 ± 0.1) nm (Fig. 6c), but the network formed by xanthan chains remained. The fibers thickness ranged from $(3.0 \pm 0.5$ nm) to $(1.0 \pm 0.2$ nm) (Fig. 6d). In the presence of $CaCO_3$ (Fig. 7a) the adsorbed layer was (7 ± 1) nm thick and resembled the one observed for pure xanthan (Fig. 3a). Nevertheless, after treating with HCl the upper layer was removed, decreasing the mean thickness to (4.5 ± 0.5) nm, and many thin fibers appeared on the surface (Fig. 7b). Cross section analyses in three different spots in Fig. 7b show that the fibers are (0.9 ± 0.1) nm high (Fig. 7c). Considering that the mean thickness of a cellulose monolayer (Wiegand, Jaworek, Wegner, & Sackmann, 1997) or of isolated chains of *Sterculia striata* polysaccharide (SSP) (Dario, de Paula, Paula, Feitosa, & Petri, 2010) amounts to ~0.7 nm and that the side chains of xanthan are longer than those of cellulose or SSP, the dimensions observed in Fig. 7 might correspond to isolated xanthan chains. The rms value determined for the layer adsorbed in the presence of $CaCO_3$ decreased from $(\text{rms} = 0.6 \pm 0.1)$ to $(\text{rms} = 0.3 \pm 0.1)$ after acid treatment.

AFM images revealed that the adsorbed layer of xanthan gum onto Si/SiO_2 in the presence of calcium salts consisted of an acid resistant sublayer, where xanthan chains were like fibers highly entangled and an upperlayer, whose morphology was calcium salt dependent. The amount of fibers in the sublayers was higher when xanthan chains were in the ordered state, i.e., when insoluble salts or 100 g/L of soluble salts were used. Even when insoluble salts were used, there is always a small amount of Ca^{2+} ions that are soluble (Table 1). Such Ca^{2+} ions play an important role as chelating agents (i) at the solid–liquid interface because they link the xanthan negatively charged groups to the negatively charged silanol groups and (ii) bridging xanthan chains in solution. The effect of Ca^{2+} counterions cannot be neglected. The larger is the charge/radius ratio, the more hydrate is the anion. The hydration enthalpy values for phosphate, carbonate and sulfate are −2647 kJ/mol, −1555 kJ/mol and −1522 kJ/mol, respectively (Smith, 1977). The xanthan gum layer adsorbed in the presence of the most hydrated anion (phosphate) was the one that exposed many entangled fibers (Fig. 6a) before the treatment with HCl. Such structure might have been favored by a large amount of "hydration" water, which was removed after drying

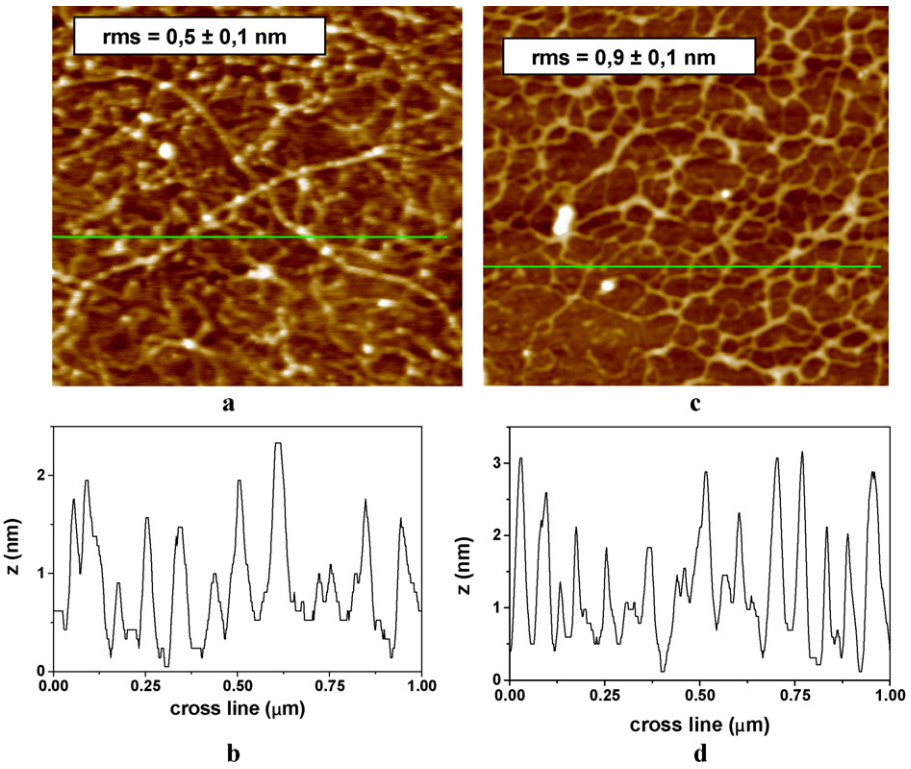

Fig. 6. Topographic AFM images (1 μm × 1 μm) obtained for xanthan layer adsorbed onto Si/SiO_2 wafers (a) in the presence of $Ca_3(PO_4)_2$ (100.0 g/L), Z = 4.0 nm with the corresponding cross section (b), (c) after rinsing with HCl, Z = 10.0 nm and (d) the corresponding cross-section.

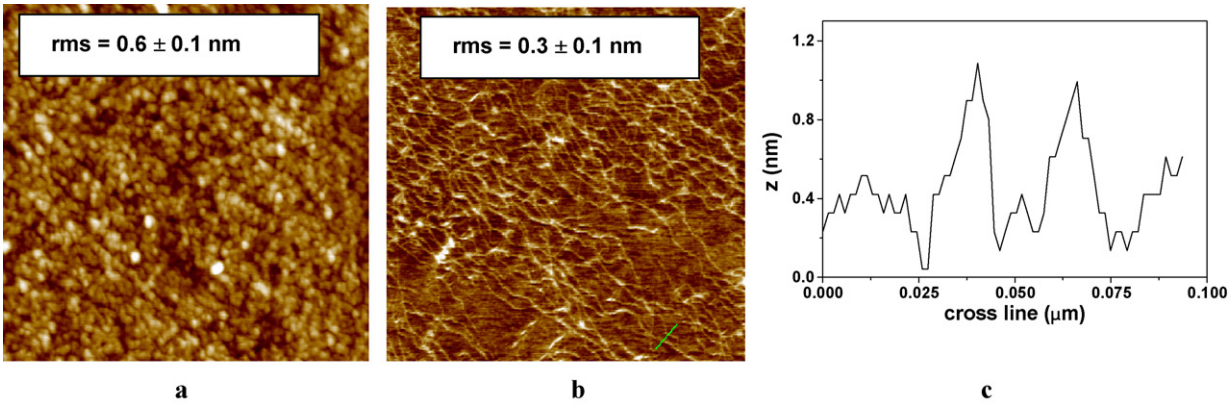

Fig. 7. Topographic AFM images (1 μm × 1 μm) obtained for xanthan layer adsorbed onto Si/SiO_2 wafers (a) in the presence of $CaCO_3$ (100.0 g/L), Z = 8.0 nm, (b) after rinsing with HCl, Z = 5.0 nm and (c) the corresponding cross-section.

under a N_2 stream. In other word, the most hydrated counter-ions might increase the size of the network "mesh". Even in the absence of salts, the hydration plays an important role in water sorption behavior of xanthan gum. Recently (Kocherbitova et al., 2010), the enthalpy of hydration of xanthan gum at zero water content was estimated as −18 kJ/mol.

4. Conclusions

Pseudoplastic behavior of xanthan gum solutions was observed in the presence of all calcium salts, regardless the concentration. The soluble salts induced the disordered state in the xanthan chains when their concentration was 1.0 g/L or 10 g/L, decreasing the K values. Nevertheless, the ordered state was recovered when the salt concentration was 100 g/L. The addition of insoluble $CaCO_3$ or $Ca_3(PO_4)_2$ particles to xanthan gum solutions led to 20% increase in the K values, when salt concentration was 100 g/L, this might be an important effect for commercial formulations. $CaSO_4$ exerted a weak effect on the flow behavior of xanthan solutions, which might be due to its lower particle density.

The adsorption behavior of xanthan gum onto a negatively charged surface such as Si/SiO_2 in the presence of calcium salts consisted of multilayers. The first adsorbed layer was formed by highly entangled xanthan chains, which is acid resistant, while the upper-layer morphology was calcium salt dependent and easily desorbed by HCl. The amount of fibers in the sublayers seems to increase at high ionic strength (ordered state) or in the presence of insoluble salts.

Acknowledgements

The authors gratefully acknowledge CNPq, FAPESP, CAPES-REDE Nanobiotec and PETROBRAS for financial support. Authors thank Leandro S. Blachechen for the SEM images.

Appendix A. Supplementary data

Supplementary data associated with this article can be found, in the online version, at doi:10.1016/j.carbpol.2010.12.047.

References

Azzam, R. M. A., & Bashara, N. M. (1987). *Ellipsometry and polarized light*. Amsterdam: North-Holland.

Barnes, H. A., Hutton, J. F., & Walters, K. (1989). *An introduction to rheology*. Amsterdam: Elsevier.

Bergmann, D., Furth, G., & Mayer, C. (2008). Binding of bivalent cations by xanthan in aqueous solution. *International Journal of Biological Macromolecules*, *43*, 245–251.

Born, K., Langendorff, V., & Boulenguer, P. (2002). Xanthan. In A. Steinbüchel, E. J. Vandamme, & S. De Baets (Eds.), *Biopolymers* (pp. 259–291). Weinheim: Wiley-VCH.

Chilingarian, G. V., & Vorabutr, P. (1981). *Drilling and drilling fluids*. New York: North-Holland.

Cuvelier, G., & Launay, B. (1986). Concentration regimes in xanthan gum solutions deduced from flow and viscosity properties. *Carbohydrate Polymers*, *6*, 321–333.

Dario, A. F., de Paula, R. C. M., Paula, H. C. B., Feitosa, J. P. A., & Petri, D. F. S. (2010). Effect of solvent on the adsorption behavior and on the surface properties of *Sterculia striata* polysaccharide. *Carbohydrate Polymers*, *81*, 284–290.

Draget, K. I., Braek, G. S., & Smidsrod, O. (1994). Alginic acid gels – The effect of alginate chemical-composition and molecular-weight. *Carbohydrate Polymers*, *25*, 31–38.

Fujimoto, J., & Petri, D. F. S. (2001). Adsorption behavior of carboxymethyl cellulose onto amino-terminated surfaces. *Langmuir*, *17*, 56–60.

Furth, G., Knierim, R., Buss, V., & Mayer, C. (2008). Binding of bivalent cations by hyaluronate in aqueous solution. *International Journal of Biological Macromolecules*, *42*, 33–40.

Geremia, R., & Rinaudo, M. (2005). Biosynthesis, structure, and physical properties of some bacterial polysaccharides. In S. Dimitriu (Ed.), *Polysaccharides: Structural diversity and functional versatility* (pp. 411–430). New York: Marcel Dekker.

Gravanis, G., Milas, M., Rinaudo, M., & Tinland, B. (1987). Comparative behavior of the bacterial polysaccharides xanthan and succinoglycan. *Carbohydrate Research*, *160*, 259–265.

Iijima, M., Shinozaki, M., Hatakeyama, T., Takahashi, M., & Hatakeyama, H. (2007). AFM studies on gelation mechanism of xanthan gum hydrogels. *Carbohydrate Polymers*, *68*, 701–707.

Kocherbitova, V., Ulvenlundb, S., Briggnerb, L.-E., Koberb, M., & Arnebrant, T. (2010). *Carbohydrate Polymers*, doi:10.1016/j.carbpol.2010.04.055.

Liu, W., Sato, T., Norisuye, T., & Fujita, H. (1987). Thermally induced conformational change of xanthan in 0,01 M aqueous sodium–chloride. *Carbohydrate Research*, *160*, 267–281.

Milas, M., Rinaudo, M., Duplessix, R., Borsali, R., & Lindner, P. (1995). Small angle neutron scattering from polyelectrolyte solutions: From disordered to ordered xanthan chain conformation. *Macromolecules*, *28*, 3119–3124.

Milas, M., Reed, W. F., & Printz, S. (1996). Conformations and flexibility of native and re-natured xanthan in aqueous solutions. *International Journal of Biological Macromolecules*, *18*, 211–221.

Mohammed, Z. H., Haque, A., Richardson, R. K., & Morris, E. R. (2007). Promotion and inhibition of xanthan 'weak-gel' rheology by calcium ions. *Carbohydrate Polymers*, *70*, 38–45.

Muller, G., Anrhourrache, M., Lecourtier, J., & Chauveteau, G. (1986). Salt dependence of the conformation of a single-stranded xanthan. *International Journal of Biological Macromolecules*, *8*, 167–172.

Neto, J. C. Q., Biscaia, E. C., Jr., & Petri, D. F. S. (2007). Adsorption behavior of polymer-based drilling fluids on SiO_2. *Química Nova*, *30*, 909–915.

Palik, E. D. (1985). *Handbook of optical constants of solids*. London: Academic Press.

Renaud, M., Belgacem, M. N., & Rinaudo, M. (2005). Rheological behaviour of polysaccharide aqueous solutions. *Polymer*, *46*, 12348–12358.

Petri, D. F. S., & Queiroz Neto, J. C. (2010). Identification of lift-off mechanism failure for salt drill-in drilling fluid containing polymer filter cake through adsorption/desorption studies. *Journal of Petroleum Science & Engineering*, *70*, 89–98.

Rosalam, S., & England, R. (2006). Review of xanthan gum production from unmodified starches by *Xanthomonas comprestris* sp. *Enzyme and Microbial Technology*, *39*, 197–207.

Smith, D. W. (1977). Ion hydration enthalpies. *Journal of Chemical Education*, *54*, 540–542.

Symes, K. C. (1980). The relationship between the covalent structure of the Xanthomonas polysaccharide (xanthan) and its function as a thickening, suspending and gelling agent. *Food Chemistry*, *6*, 63–76.

Tinland, B., & Rinaudo, M. (1989). Dependence of the stiffness of the xanthan chain on the external salt concentration. *Macromolecules*, *22*, 1863–1865.

Weast, R. C. (Ed.). (1983–1984). *CRC handbook of chemistry and physics*. Boca Raton, FL: CRC Press Inc.

Wiegand, G., Jaworek, T., Wegner, G., & Sackmann, E. (1997). Heterogeneous surfaces of structured hairy-rod polymer films: Preparation and methods of functionalization. *Langmuir*, *13*, 3563–3569.

Xie, W., & Lecourtier, J. (1992). Xanthan behaviour in water-based drilling fluids. *Polymer Degradation and Stability*, *38*, 155–164.